Emergent constraint on Arctic Ocean acidification in the twenty-first century

Jens Terhaar[1,2,3*], Lester Kwiatkowski [1,4], Laurent Bopp[1]

[1] LMD/IPSL, Ecole Normale Supérieure/PSL Université, CNRS, Ecole Polytechnique, Sorbonne Université, Paris, France

[2] Climate and Environmental Physics, Physics Institute, University of Bern, Switzerland

[3] Oeschger Center for Climate Change Research, University of Bern, Switzerland

[4] LOCEAN/IPSL, Sorbonne Université, CNRS, IRD, MNHN, Paris, France

***Jens Terhaar**

Climate and Environmental Physics, Physics Institute

University of Bern

Sidlerstrasse 5

3012 Bern

Switzerland

jens.terhaar@climate.unibe.ch

The ongoing uptake of anthropogenic carbon by the ocean leads to ocean acidification, a process that results in a reduction in pH and the saturation state of biogenic calcium carbonate minerals ($\Omega_{calc/arag}$)[1,2]. Due to naturally low $\Omega_{calc/arag}$[2,3], the Arctic Ocean is considered the most susceptible region to future acidification and associated ecosystem impacts[4,5,6,7]. However, the magnitude of projected twenty-first century acidification differs strongly across Earth System Models (ESMs)[8]. Here we identify an emergent multi-model relationship between the simulated present-day density of Arctic Ocean surface waters, used as a proxy for Arctic deep-water formation, and projections of the anthropogenic carbon inventory and coincident acidification. Applying observations of sea surface density, we constrain the end of twenty-first century Arctic Ocean anthropogenic carbon inventory to 9.0 ± 1.6 Pg C and basin-averaged Ω_{arag} and Ω_{calc} to 0.76 ± 0.06 and 1.19 ± 0.09 respectively, under the RCP 8.5 climate scenario. Our results indicate greater regional anthropogenic carbon storage and ocean acidification than previously projected[3,8] and increase the probability that large parts of the mesopelagic Arctic Ocean will be undersaturated with respect to calcite by the end of the century. This increased rate of Arctic Ocean acidification combined with rapidly changing physical and biogeochemical Arctic conditions[9,10,11], is likely to exacerbate the impact of climate change on vulnerable Arctic marine ecosystems.

While the uptake of atmospheric carbon by the ocean mitigates climate change, it also dramatically influences marine chemistry, decreasing pH and carbonate ion concentrations [CO_3^{2-}] and increasing concentrations of aqueous carbon dioxide and bicarbonate ions [HCO_3^-][1,2]. These changes in seawater chemistry, collectively known as ocean acidification, have been shown to negatively impact wide-ranging marine organisms including molluscs, crustaceans, echinoderms, cnidarians and teleost fish[4,5,6,7]. Calcifying marine organisms are particularly sensitive to ocean acidification, which can impair their growth, reproduction and survival[2,4,12]. The thermodynamic stability of calcium carbonate is described by the calcium carbonate saturation state ($\Omega = [Ca^{2+}][CO_3^{2-}]/K_{sp}$), with K_{sp} representing the relevant $CaCO_3$ solubility product, and Ω_{calc} and Ω_{arag} representing the saturation state of the stable calcite and metastable aragonite mineral forms, respectively. Ocean acidification acts to reduce Ω by reducing carbonate ion concentrations. Studies have shown that as Ω decreases, calcification rates at both the organism[12,13,14] and community-level[15] typically decline. In addition, the corrosion of pure mineral forms is actively promoted under exposure to undersaturated conditions ($\Omega<1$).

The Arctic represents the global region projected to experience the most severe climate change, with polar amplification causing a projected end-of-century surface temperature increase of up to 8.3±1.9 °C[10] and loss of summer sea-ice[11]. The same is true for the Arctic Ocean, where low temperatures and consequently the high solubility of CO_2, result in naturally low pH and Ω[2,3]. Given this natural state and the amplifying effect of climate change[16], the Arctic Ocean is projected to experience the lowest pH and Ω conditions in the coming decades[3], as well as dramatic changes in the temporal variability of marine chemistry[9].

Projections by ESMs under the high-emissions Representative Concentration Pathway 8.5 (RCP8.5)[17] suggest that the entire Arctic Ocean will be undersaturated with respect to aragonite ($\Omega_{arag}<1$) by the end of the twenty-first century (Fig. 1), while basin-wide calcite undersaturation ($\Omega_{calc}<1$) is not expected to occur this century[3,8,18] (Extended Data Figure 1). Projected changes in ocean chemistry are predominantly confined to the upper 2500 m of the water column, with large model uncertainties persisting with regard to the end-of-century anthropogenic carbon inventory (2.9-13.0 Pg C)[19], and the associated average Ω_{arag} (0.66-0.95) and Ω_{calc} (1.02-1.49)[8]. Although projection uncertainties are limited in the surface ocean[20], they are highly pronounced at depth (Fig. 1 and Extended Data Figure 1) and complicate assessments of likely impacts on vulnerable marine ecosystems[7].

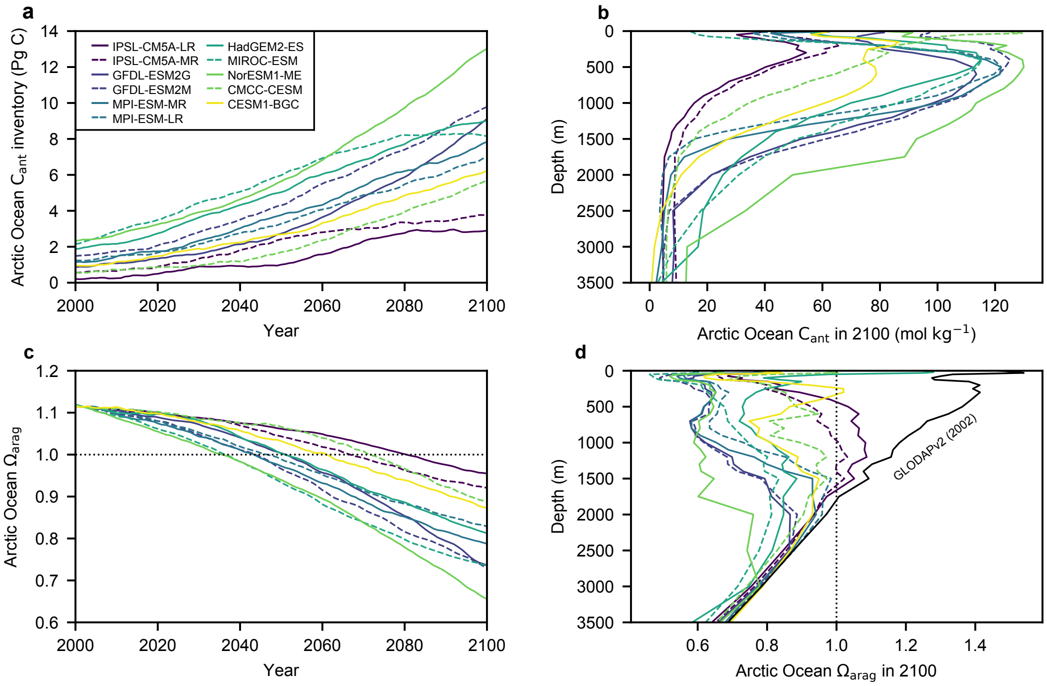

Fig. 1. Projections of Arctic Ocean anthropogenic carbon and aragonite saturation state. a, ESM projections of the twenty-first century Arctic Ocean anthropogenic carbon (C_{ant}) inventory and **c**, basin-averaged Ω_{arag}. Vertical profiles of **b**, basin-averaged anthropogenic carbon and **d**, Ω_{arag} in 2100 for the 11 ESMs. The GLODAPv2[24] observational profile of Ω_{arag} for 2002 is marked as a black line in **d**. Arctic Ocean boundaries are the Fram Strait, the Barents Sea Opening, the Bering Strait and the Canadian Arctic Archipelago.

To reduce Arctic Ocean projection uncertainties associated with the anthropogenic carbon inventory and concurrent acidification, here we utilise the recent approach of emergent constraints[11,21,22,23]. In order to constrain future ESM projection uncertainties, emergent constraints relate long-timescale climate sensitivities and impacts to observable properties, such as short-timescale climate variability or trends, across ESM ensembles. Emergent constraints have previously been used to reduce the uncertainty, amongst other climate projections, associated with Arctic summer sea ice[11], equilibrium climate sensitivity[22] and impacts on marine primary production[21].

Here we show that across an ensemble of 11 ESMs (Table S1) there is a consistent relationship between present-day Arctic Ocean maximum sea surface water density, the projected end-of-century Arctic Ocean anthropogenic carbon inventory and the extent of ocean acidification under RCP8.5 (Fig. 2, 3). All models performed simulations as part of the Coupled Model Intercomparison Project Phase 5 (CMIP5). Present-day (1986-2005) maximum sea surface density was calculated, for each model, as the mean of the 95th percentile of monthly surface water densities in the Arctic. Across all models, these maximum density waters are primarily located in the Barents Sea (Extended Data Figure 2). The anthropogenic carbon inventory was calculated as the difference in integrated Arctic Ocean dissolved inorganic carbon between RCP8.5 simulations and the respective pre-industrial control simulation of each model. While projections of variables associated with ocean acidification ($\Omega_{calc/arag}$, pH and pCO$_2$) were calculated from model outputs of total alkalinity, dissolved inorganic carbon, temperature, salinity, total dissolved inorganic phosphorus and silicon and bias-corrected using GLODAPv2[24] (see Methods).

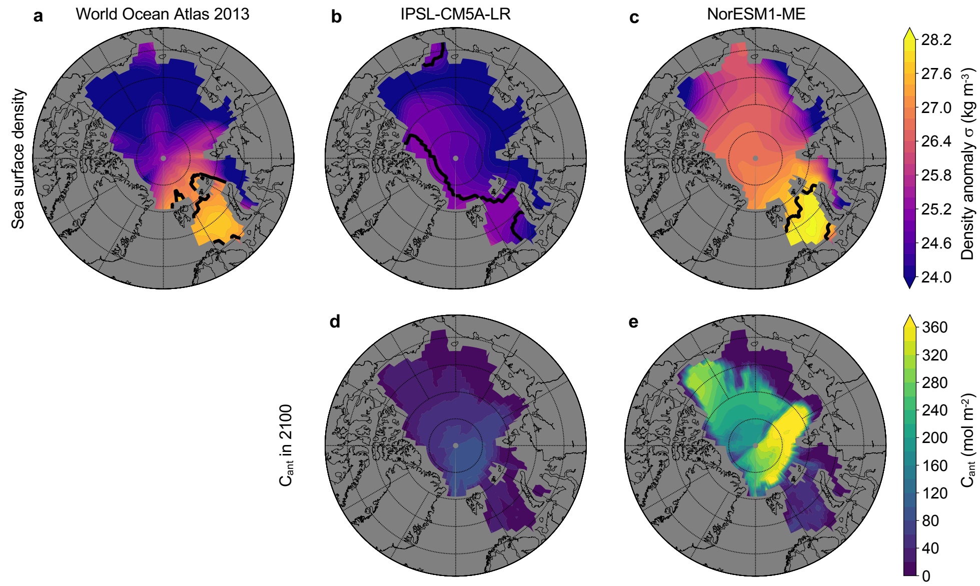

Fig. 2. Arctic Ocean surface water density and the anthropogenic carbon inventory. a, Present-day annual-mean sea surface density from World Ocean Atlas 2013[25] and the **b**, IPSL-CM5A-LR and **c**, NorESM1-ME models. Contours delineate regions that contribute to the maximum surface density as defined by the 95th percentile densities. Vertically integrated anthropogenic carbon (C_{ant}) projections in 2100 for the **d**, IPSL-CM5A-LR and **e**, NorESM1-ME models. IPSL-CM5A-LR represents the ensemble minimum for both present-day maximum sea surface density (1025.67 kg m^{-3}) and projected C_{ant} inventory in 2100 (2.9 Pg C), while NorESM1-ME is the ensemble maximum (1028.24 kg m^{-3} and 13.0 Pg C). The maximum sea surface density from WOA 2013 is 1027.85 kg m^{-3}

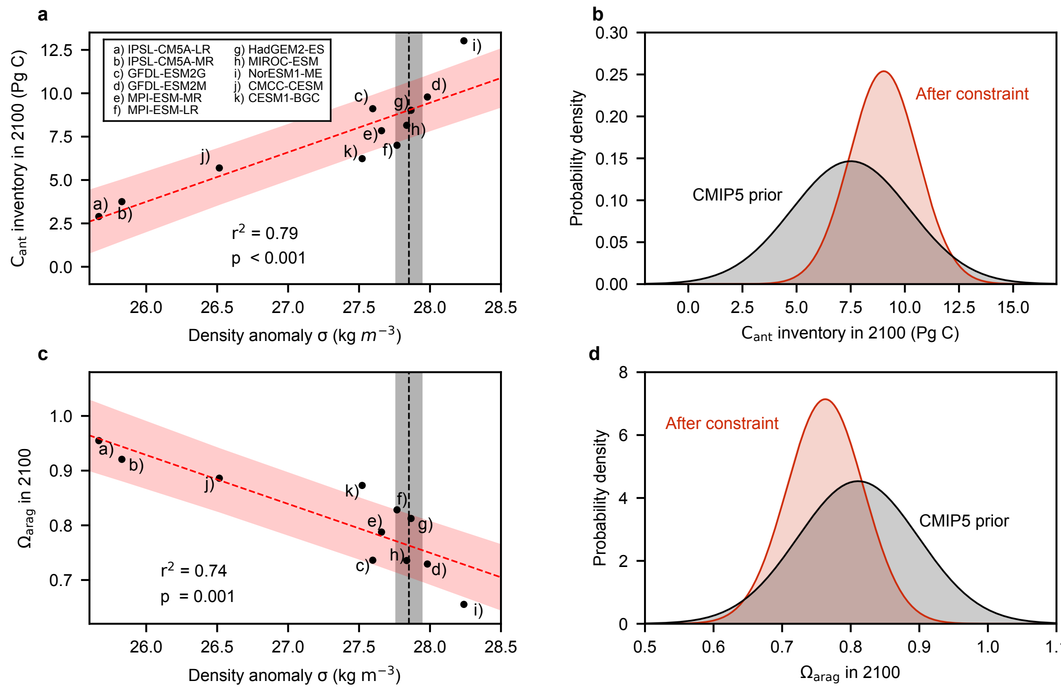

Fig. 3. Emergent constraints on the projected anthropogenic carbon inventory and future acidification. **a**, The projected Arctic Ocean anthropogenic carbon inventory and **c**, basin-averaged Ω_{arag} in 2100 against present-day maximum sea surface density (95th percentile waters) for the ESM ensemble (black dots). Linear regression fits (red dashed lines) and the associated 68 % prediction intervals are shown, as are data-based estimates of present-day maximum sea surface density (black dashed lines) with the associated standard deviation (black shaded area). Probability density functions for the end-of-century **b**, Arctic Ocean anthropogenic carbon inventory and **d**, basin-averaged Ω_{arag}, before (black) and after (red) the emergent constraint is applied.

ESMs such as IPSL-CM5A-LR, which simulate lower than observed present-day Arctic Ocean maximum surface densities, a proxy for Arctic deep-water formation (Extended Data Figure 3), typically project lower end-of-century anthropogenic carbon inventories under RCP8.5 than models such as NorESM1-ME, which simulate higher densities (Fig. 2). This emergent relationship across the ESM ensemble is consistent at the scale of the Arctic Ocean basin, with present-day maximum surface density exhibiting a strong relationship with end-of-century depth integrated anthropogenic carbon inventories (r^2=0.79, $P < 0.001$; Fig. 3). Given the dominance of anthropogenic carbon uptake in driving ocean acidification (Extended Data Figure 4), models with higher maximum sea surface density also exhibit stronger twenty-first century reductions in basin-average Ω_{arag} (r^2=0.74, $P = 0.001$; Fig. 3), Ω_{calc} (r^2=0.74, $P = 0.001$; Extended Data Figure 1) and pH (r^2=0.77, $P < 0.001$; Extended Data Figure 1). Observations of sea surface density[25] were then used in combination with these multi-model relationships, to provide emergent constraints on projections of Arctic Ocean anthropogenic carbon storage, and concomitant acidification. Potential alternative constraints, such as present-day seasonal sea ice extent, were found to be non-indicative of future Arctic Ocean anthropogenic carbon and acidification across the ESM ensemble (Extended Data Figure 3).

Our emergent constraint increases projections of the end-of-century Arctic Ocean anthropogenic carbon inventory from 7.5 ± 2.7 Pg C (CMIP5 multi-model mean) to 9.0 ± 1.6 Pg C, with a 41 % reduction in uncertainty (Fig. 3). Similarly, average end-of-century Ω_{arag} and Ω_{calc} are reduced from 0.81 ± 0.09 to 0.76 ± 0.06 and from 1.27 ± 0.14 to 1.19 ± 0.09, respectively (Fig. 3, Extended

Data Figure 1). As such, the low bias of maximum sea surface density in 8 of 11 ESMs is indicative of an underestimation of projected anthropogenic carbon storage and therefore future Arctic Ocean acidification in the CMIP5 multi-model mean.

The mechanisms underpinning the relationship between maximum surface densities and anthropogenic carbon uptake are intrinsically related to Arctic Ocean circulation and dynamics. The majority of intermediate and deep Arctic waters and the anthropogenic carbon they carry are of Atlantic origin[26,27]. The dominant net influx of anthropogenic carbon from the Atlantic into the Arctic Ocean is through the Barents Sea Opening, as indicated by both data-based estimates[28] (41 ± 8 Tg C yr^{-1}) and ocean carbon cycle models (21-48 Tg C yr^{-1}; Table S2). This inflowing water is seasonally cooled in the Barents Sea via surface heat exchange and enriched in salinity via brine rejection during the formation of sea ice[29,30]. Consequently, during winter, seawater density increases and water masses sink into the interior Arctic Ocean, mainly via the St Anna Trough, where they supply most intermediate and deep waters[26,27]. As such, the present-day ability of ESMs to simulate the maximum surface densities that occur in the Barents Sea, is highly indicative of their capacity to transport future anthropogenic carbon into the Arctic interior.

These mechanisms were further explored in historical (1870-2012) simulations of an ocean-only carbon-cycle model (NEMO-PISCES), performed at three spatial resolutions[19]. These simulations confirm the importance of Atlantic waters that flow into the Barents Sea, in determining net changes in the Arctic Ocean anthropogenic carbon inventory (Table S2). They further show that across model spatial resolutions there is a strong positive relationship (r^2=0.98, P = 0.08; Fig. S1) between maximum surface density and the historical change in Arctic Ocean anthropogenic carbon inventory (Fig. S2). One of the principal drivers of the CMIP5 emergent relationship therefore appears to be variable ESM resolution and associated difficulties in resolving the transport of anthropogenic carbon into the Arctic basin at low resolutions[19]. Indeed, CMIP5 ESMs with higher Arctic Ocean resolution typically project greater end-of-century anthropogenic carbon inventories (r^2=0.44, P = 0.03; Extended Data Figure 3).

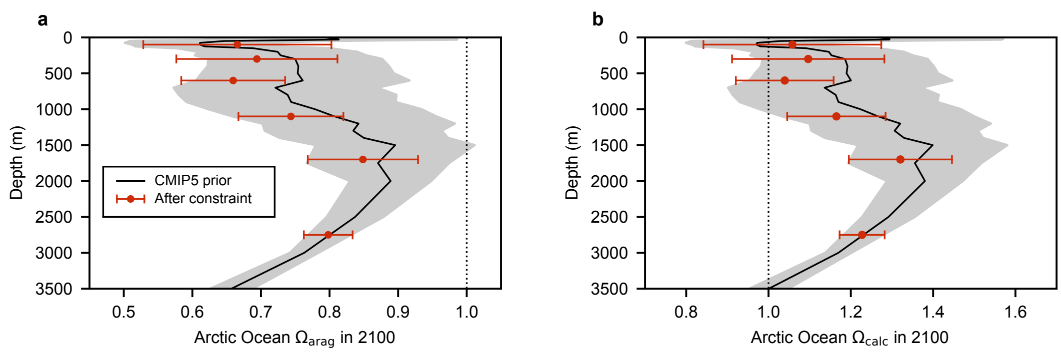

Fig. 4. Constrained end-of century Arctic Ocean vertical profiles of $\Omega_{calc/arag}$. Multi-model mean vertical profiles of basin-averaged **a**, Ω_{arag} and **b**, Ω_{calc} in 2100 (black lines) with the associated standard deviation (n=11; grey shading). Constrained mean estimates of Ω_{arag} and Ω_{calc} (red dots) are shown for six different depth layers (0-200 m, 200-400 m, 400-800 m, 800-1400 m, 1400-2000 m, 2000 m - bottom). The constrained estimates are shown at the mid-point of each layer, with error bars representing ± one standard deviation.

Extending the emergent constraint approach from the entire Arctic basin to multiple vertical depth integrals, we reduce uncertainties associated with projections of changing vertical profiles of $\Omega_{calc/arag}$ (Fig. 4, Extended Data Figures 5, 6), pH and pCO$_2$ (Extended Data Figures 7, 8). Basin-wide emergent constraints on twenty-first century acidification are shown to be predominantly driven by subsurface waters between 400 and 1400 m, with the strongest multi-model relationship between present-day maximum surface density and end-of-century $\Omega_{calc/arag}$ found between 400 and 800 m (r^2 = 0.84, P<0.001; Extended Data Figures 5, 6). In these mesopelagic waters, end-of-century Ω_{arag} is reduced from a CMIP5 multi-model mean of 0.75 ± 0.15 to 0.66 ± 0.08, with end-of-century Ω_{calc} reduced from 1.18 ± 0.23 to 1.04 ± 0.12. A consequence of our constrained vertical profiles of marine chemistry is that the lowest average end-of-century $\Omega_{calc/arag}$ will likely not occur in Arctic Ocean surface waters, as previously expected[3,8], but between 400-800 m (Fig. 4). In these mesopelagic waters, the probability of end-of-century Ω_{calc} < 1 and Ω_{arag} < 0.75 is increased from 23% and 51% respectively in the CMIP5 prior to 37% and 88% respectively after the constraint is applied (Extended Data Table 1).

In the upper Arctic Ocean (0-200 m), present-day maximum surface density exhibits limited relationship with end-of-century $\Omega_{calc/arag}$ across the models (Extended Data Figures 5, 6) and emergent constraints offer no reduction in projection uncertainties (Fig. 4). This is to be expected in waters where deep-water formation has little impact on marine chemistry. Similarly, below 2000 m where there is limited change in the anthropogenic carbon inventory and associated marine chemistry this century (Fig. 1, Extended Data Figure 1), there is no relationship between present-day maximum surface density and end-of-century $\Omega_{calc/arag}$ (Extended Data Figures 5, 6).

The constrained estimates of greater twenty-first century Arctic Ocean acidification presented here, have major implications for sensitive Arctic marine ecosystems already exposed to multiple climatic stressors. Enhanced subsurface acidification is likely to have negative consequences on organisms that both permanently inhabit the mesopelagic and those that utilise it as part of seasonal or diel vertical migrations[31]. The suitable habitat available to keystone species such as the aragonitic pteropod *Limacina helicina* is likely to decline to a greater extent than previously anticipated given its sensitivity to Ω_{arag}[32], with negative consequences for dependent pelagic food webs[33,34,35]. Meanwhile, undersaturation with respect to calcite is likely to have major consequences for calcite forming Arctic coccolithophores[36] and foraminifera[37]. Finally, our estimates of higher end-of century Arctic Ocean pCO_2, which increases from 1070 ± 239 µatm at depths of 400-800 m to 1216 ± 121 µatm under the constraint (Extended Data Figure 8), is likely to negatively affect the growth, survival[38] and behaviour[39,40] of ecologically important fish such as polar cod.

References

1. Haugan, P. M. & Drange, H. Effects of CO_2 on the ocean environment. *Energy Convers. Mgmt* **37**, 1019–1022 (1996).

2. Orr, J. C. et al. Anthropogenic ocean acidification over the twenty-first century and its impact on calcifying organisms. *Nature* **437**, 681–686 (2005).

3. Steinacher, M., Joos, F., Frolicher, T. L., Plattner, G. K. & Doney, S. C. Imminent ocean acidification in the Arctic projected with the NCAR global coupled carbon cycle-climate model. *Biogeosciences* **6**, 515–533 (2009).

4. Fabry, V. J., McClintock, J. B., Mathis, J. T. & Grebmeier, J. M. Ocean acidification at high latitudes: The bellweather. *Oceanography* **22**, 160–171 (2009).

5. Gattuso, J.-P. & Hansson, L. *Ocean Acidification* (Oxford Univ. Press, 2011).

6. Riebesell U, Gattuso JP, Thingstad TF, Middelburg JJ. Preface “Arctic ocean acidification: pelagic ecosystem and biogeochemical responses during a mesocosm study”. *Biogeosciences* **10**(8), 5619–5626 (2013).

7. AMAP, 2018. AMAP Assessment 2018: Arctic Ocean Acidification. Arctic Monitoring and Assessment Programme (AMAP), Tromsø, Norway. vi+187pp

8. Steiner, N. S., Christian, J. R., Six, K. D., Yamamoto, A., & Yamamoto-Kawai, M. Future ocean acidification in the Canada Basin and surrounding Arctic Ocean from CMIP5 earth system models. *Journal of Geophysical Research: Oceans* **119**(1), 332–347 (2014).

9. Kwiatkowski, L. & Orr, J.C. Diverging seasonal extremes for ocean acidification during the twenty-first century. *Nature Climate Change* **8**(2), 141 (2018)

10. Collins, M. et al. in *Climate Change 2013: The Physical Science Basis* (eds Stocker, T. F. et al.) 1029–1136 (IPCC, Cambridge Univ. Press, 2013).

11. Boé, J., Hall, A. & Qu, X. September sea ice cover in the Arctic Ocean projected to vanish by 2100. *Nature Geosci.* **2**, 341–343 (2009).

12. Kroeker, K. J., Kordas, R. L., Crim, R. N. & Singh, G. G. Meta-analysis reveals negative yet variable effects of ocean acidification on marine organisms. *Ecol. Lett.* **13**, 1419–1434 (2010).

13. Langdon, C. & Atkinson, M. Effect of elevated pCO_2 on photosynthesis and calcification of corals and interactions with seasonal change in temperature/irradiance and nutrient enrichment. *J. Geophys. Res.* **110**, C09S07 (2005).

14. Bednaršek, N., Tarling, G. A., Bakker, D. C., Fielding, S. & Feely, R. A. Dissolution dominating calcification process in polar pteropods close to the point of aragonite undersaturation. *PLoS ONE* **9**(10), e109183 (2014).

15. Albright, R. et al. Reversal of ocean acidification enhances net coral reef calcification. *Nature* **531**, 362–365 (2016).

16. Yamamoto-Kawai, M., McLaughlin, F. A., Carmack, E. C., Nishino, S. & Shimada, K. Aragonite undersaturation in the Arctic Ocean: Effects of ocean acidification and sea ice melt. *Science* **326**, 1098–1100 (2009).

17. Riahi, K. et al. RCP 8.5—A scenario of comparatively high greenhouse gas emissions. *Clim. Change* **109**, 33–57 (2011).

18. Feely, R. A., Doney, S. C. & Cooley, S. R. Ocean acidification: Present conditions and future changes in a high-CO_2 world. *Oceanography* **22**, 36–47 (2009).

19. Terhaar, J., Orr, J. C., Gehlen, M., Ethé, C., and Bopp, L. Model constraints on the anthropogenic carbon budget of the Arctic Ocean. *Biogeosciences* **16**, 2343–2367 (2019).

20. Frolicher, T. L., Rodgers, K., Stock, C. & Cheung, W. W. L. Sources of uncertainties in 21st century projections of potential ocean ecosystem stressors. Global Biogeochem. Cycles 30, 1224–1243 (2016).

21. Kwiatkowski, L. et al. Emergent constraints on projections of declining primary production in the tropical oceans. *Nat. Clim. Chang.* **7**, 355–358 (2017).

22. Cox, P. et al. Sensitivity of tropical carbon to climate change constrained by carbon dioxide variability. *Nature* **494**, 341–344 (2013)

23. Eyring, V. et al. Taking climate model evaluation to the next level. *Nat. Clim. Chang.* **9**, 102–110 (2019).

24. Lauvset, S. K. et al. A new global interior ocean mapped climatology: the 1°×1° GLODAP version 2. *Earth Syst. Sci. Data* **8**, 325–340 (2016).

25. Boyer, T. P. et al. *World Ocean Database 2013* (Silver Spring, accessed March 2019).

26. Rudels, B., Jones, E. P., Anderson, L. G., & Kattner, G. On the intermediate depth waters

of the Arctic Ocean. *The polar oceans and their role in shaping the global environment*, **85**, 33-46 (1994).

27. Rudels, B., Muench, R. D., Gunn, J., Schauer, U., & Friedrich, H. J. Evolution of the Arctic Ocean boundary current north of the Siberian shelves. *J. Marine Syst.*, **25**(1) . (2001). 77-99.

28. Jeansson, E. et al. The Nordic Seas carbon budget: Sources, sinks, and uncertainties. *Global Biogeochem, Cy.*, **25**(4). (2011)

29. Midttun, Lars. "Formation of dense bottom water in the Barents Sea." *Deep Sea Res.* **32**.10, 1233-1241 (1985)

30. Smedsrud, L. H. et al. The role of the Barents Sea in the Arctic climate system. R*ev. Geophys.* **51**, 415–449 (2013).

31. Berge, J. et al. In the dark: A review of ecosystem processes during polar night. *Prog. Oceanogr.* **139**, 258–271 (2015).

32. Comeau, S., Jeffree, R., Teyssie, J. L. & Gattuso, J. P. Response of the Arctic pteropod Limacina helicina to projected future environmental conditions. *PLoS ONE* **5**, e11362 (2010).

33. Hunt, B. P. V. et al. Pteropods in Southern Ocean ecosystems. *Prog. Oceanogr.* **78**, 193–221 (2008).

34. Armstrong, J. L. et al. Distribution, size, and interannual, seasonal and diel food habits of northern Gulf of Alaska juvenile pink salmon, Oncorhynchus gorbuscha. *Deep-Sea Res. Pt. II* **52**, 247–265 (2005).

35. Karnovsky, N. J., Hobson, K. A., Iverson, S., & Hunt Jr, G. L. Seasonal changes in diets of seabirds in the North Water Polynya: a multiple-indicator approach. *Mar. Ecol. Prog. Ser.*, **357**, 291–299 (2008).

36. Kottmeier, D. M., Rokitta, S. D., & Rost, B. H^+-driven increase in CO_2 uptake and decrease in HCO^-_3 uptake explain coccolithophores' acclimation responses to ocean acidification. *Limnol. Oceanogr.* **61**, 2045–2057 (2016)

37. Davis, C. V. et al. Ocean acidification compromises a planktic calcifier with implications for global carbon cycling. *Sci. Rep.* **7**, 2225 (2017)

38. Frommel, A. Y. et al. Severe tissue damage in Atlantic cod larvae under increasing ocean acidification. *Nature Clim. Change* **2**, 42–46 (2012).

39. Schmidt, M. et al. Differences in neurochemical profiles of two gadid species under ocean warming and acidification. *Front. Zool.* **14**, 49 (2017).

40. Kunz, K. et al. Aerobic capacities and swimming performance of polar cod (Boreogadus saida; lepechin) under ocean acidification and warming conditions. *J. Exp. Biol*. **221** (2018)

Methods

Earth System Models

In the ensemble of 11 Coupled Model Intercomparison Project Phase 5 (CMIP5) ESMs (Table S1) utilised, all included coupled ocean biogeochemistry schemes and have been extensively applied within the context of both climate and ocean biogeochemical projections[8,9,21]. A single ensemble member was utilised for each ESM. Prognostic annual model output fields of dissolved inorganic carbon, total alkalinity, dissolved inorganic phosphorus and silicon, temperature, and salinity were taken across all vertical depth levels in the Arctic Ocean, limited by the Fram Strait, the Barents Sea Opening, the Bering Strait and the Canadian Arctic Archipelago[19,41]. Monthly sea surface density outputs were taken over the same domain. All output fields were regridded on a regular 1°×1° grid to facilitate multi-model analysis.

The anthropogenic carbon inventory was calculated as the difference between dissolved inorganic carbon in historical (1850-2005) simulations merged with RCP8.5 (2006-2100) and the concurrent pre-industrial control (piControl) simulations. As such, any model drift in deep-ocean dissolved inorganic carbon was directly accounted for. Across all models, the simulated present-day (2005) Arctic Ocean anthropogenic carbon inventory (0.2-2.4 Pg C) is below the data-based estimate of 2.5-3.3 Pg C[42].

All carbonate chemistry variables were calculated offline from dissolved inorganic carbon, total alkalinity, temperature, salinity and where available, dissolved inorganic phosphorus and silicon, over 1850-2100 using mocsy2.0[43] and the equilibrium constants recommended for best practices[44]. To account for carbonate chemistry biases in the present-day mean state of the ESMs[8], model anomalies of all input variables relative to 2002 were combined with the data-based GLODAPv2 observational product[24] which is normalised to the year 2002. Model anomalies were corrected for potential model drift using concurrent piControl simulations. All grid cells with GLODAPv2 observational coverage (~65 % of Arctic Ocean volume) were utilised. Basin-wide averages of Ω_{arag}, Ω_{calc}, pH and $p\mathrm{CO_2}$ were weighted based on grid cell volumes.

The Arctic Ocean present-day maximum sea surface density was calculated for each ESM from 1986-2005 monthly sea surface density climatologies, constructed from temperature and salinity outputs. Maximum present-day sea surface density was defined as the mean density of the densest 5 % of Arctic surface waters (95th percentile waters) throughout the climatological year. Maximum present-day sea surface density consistently occurs in the Barents Sea, across both observations and the ESM ensemble. Given the importance of the Barents Sea in supplying intermediate and deep Arctic waters[26,27,29,30], maximum sea surface density, as defined, is indicative of the bowl of ventilated Arctic waters. Across all models, the volume of Arctic Ocean waters that are lighter than the maximum sea surface density increases with the maximum sea surface density ($r^2 = 0.59$, $P=0.006$; Extended Data Figure 3).

In addition to sea surface density, alternative potential constraints on the projected Arctic Ocean anthropogenic carbon inventory and associated acidification were assessed. The representation of Arctic sea ice extent[45] and intermediate North Atlantic water masses[46] varies substantially across the CMIP5 ensemble. However, both present-day sea-ice extent (Extended Data Figure 3) and the properties of North Atlantic water masses were found to be non-indicative of projected Arctic Ocean carbon uptake and associated acidification across the model ensemble.

An assessment of the potential for model internal variability to influence the Arctic Ocean emergent constraint approach is provided in the supplementary material. Utilising four ensemble members of the IPSL-CM5A-LR model, the internal variability of present-day sea surface density and projected anthropogenic carbon inventory is shown to be highly limited compared to the differences across the CMIP5 models (Extended Data Figure 9).

Ocean-only simulations

Hindcast ocean-biogeochemical simulations of the NEMO-PISCES model[47] that have been previously published[19] are used in this study to explore the mechanisms behind the identified Arctic Ocean emergent constraint. The model is run at a nominal resolution of 0.5° from 1870 to 1958 and at three different nominal horizontal resolutions from 1958 to 2012: 2° (ORCA2), 0.5° (ORCA05), and 0.25° (ORCA025). All three model configurations are forced with the DRAKKAR historical reanalysis forcing dataset[48] and therefore only differ in horizontal resolution and the associated diffusion scheme and coefficients.

Observational constraints

Observational sea surface density constraints were derived from the World Ocean Atlas 2013 temperature and salinity climatologies[25]. The maximum Arctic Ocean sea surface density was then calculated in the same manner as for the ESM ensemble.

The uncertainty associated with Arctic Ocean maximum sea surface density observational constraints was estimated using standard propagation of uncertainty and combining (1) the published standard deviations of sea surface temperature and salinity for each grid cell and each month in WOA2013 to derive standard deviations for sea surface density, and (2) the standard deviation obtained when computing the weighted mean of 95th percentile density waters.

Arctic Ocean salinity in World Ocean Atlas 2013 was recently evaluated against available in-situ data[49]. This comparison suggests that salinity observations in the World Ocean Atlas may have a small negative bias in the Barents Sea that may contribute to a negative density bias. Corroboration and correction of such a bias would, if anything, result in a minor increase in our constrained estimates of projected Arctic Ocean anthropogenic carbon and associated acidification.

Probability density functions of anthropogenic carbon and ocean acidification

Probability density functions (PDFs) of anthropogenic carbon storage and basin-averaged Ω_{arag}, Ω_{calc} and pH in 2100 were calculated for the unconstrained (prior) CMIP5 ensemble and the emergent constraints. The prior PDF was derived assuming all models were equally likely and sampled from a Gaussian distribution. The constrained PDFs were calculated as the normalised product of the conditional PDF of the emergent relationship and the PDF of the observational constraint following previously established methodologies[21,22,50].

References (Methods)

41. Bates, N. R. & Mathis, J. T. The Arctic Ocean marine carbon cycle: Evaluation of air-sea CO2 exchanges, ocean acidification impacts and potential feedbacks. *Biogeosciences* **6**, 2433–2459 (2009).

42. Tanhua, T. et al. Ventilation of the Arctic Ocean: mean ages and inventories of anthropogenic CO2 and CFC-11. J. Geophys. Res. 114 (2009).

43. Orr, J. C. & Epitalon, J.-M. Improved routines to model the ocean carbonate system: mocsy 2.0. *Geosci. Model Dev.* **8**, 485–499 (2015).

44. Dickson, A. G., Sabine, C. L. & Christian, J. R. (eds) *Guide to Best Practices For Ocean CO2 Measurements*191 (PICES Special Publication 3, 2007).

45. Shu, Q., Song, Z. & Qiao, F. Assessment of sea ice simulations in the CMIP5 models. *Cryosphere* **9**, 399–409 (2015).

46. Shu, Q., Wang, Q., Su, J., Li, X., & Qiao, F. Assessment of the Atlantic water layer in the Arctic Ocean in CMIP5 climate models. *Clim. Dyn.* **53** 5279-5291 (2019).

47. Aumont, O. & Bopp, L. Globalizing results from ocean in situ iron fertilization studies. *Glob. Biogeochem. Cycles* **20**, GB2017 (2006).

48. Brodeau, L., Barnier, B., Treguier, A. M., Penduff, T. & Gulev, S. An ERA40-based atmospheric forcing for global ocean circulation models. *Ocean Model.* **31**, 88–104 (2010).

49. Xie, J., Raj, R. P., Bertino, L., Samuelsen, A., & Wakamatsu, T. Evaluation of Arctic Ocean surface salinities from SMOS and two CMEMS reanalyses against in situ data sets. Ocean Sci. 15,

1191–1206 (2019).

50. Wenzel, S., Cox, P. M., Eyring, V. & Friedlingstein, P. Emergent constraints on climate-carbon cycle feedbacks in the CMIP5 Earth system models. *J. Geophys. Res. Biogeosciences* **119**, 2013JG002591 (2014).

Acknowledgements

This study was funded by the H2020 C-CASCADES grant (ref 643052), the H2020 CRESCENDO grant (ref 641816), the H2020 4C grant (ref 821003), the Agence Nationale de la Recherche grant ANR-18-ERC2-0001-01 (CONVINCE), the MTES/FRB Acidoscope project and the ENS-Chanel research chair. We acknowledge the World Climate Research Programme's Working Group on Coupled Modelling, which is responsible for CMIP. For CMIP the US Department of Energy's Program for Climate Model Diagnosis and Intercomparison provided coordinating support and led the development of software infrastructure in partnership with the Global Organisation for Earth System Science Portals. The authors also thank the IPSL modelling group for the software infrastructure, which facilitated CMIP5 analysis, Jean-Marc Molines, Laurent Brodeau, and Bernard Barnier for developing the DRAKKAR ORCA05 and ORCA025 global configurations of NEMO and Jennifer Simeon, Christian Ethé, Marion Gehlen, and James C. Orr for the implementation of NEMO-PISCES within these configurations.

Author contributions

This study was conceived by all coauthors. J.T. performed the model output analysis and produced the figures, with help from L.K. and L.B. All authors contributed ideas, discussed the results and wrote the manuscript.

Author information

The authors declare no competing financial interests. Correspondence and requests for materials should be addressed to J.T (jens.terhaar@climate.unibe.ch).

Data availability

The Earth system model output used in this study is available via the Earth System Grid Federation (https://esgf-node.ipsl.upmc.fr/projects/esgf-ipsl/). Observations from the World Ocean Atlas 2013 (https://www.nodc.noaa.gov/OC5/woa18/) and GLODAPv2 (https://www.nodc.noaa.gov/ocads/oceans/GLODAPv2_2019/) are available via the National Oceanic and Atmospheric Administration. Prior to publication, the output of ocean-only NEMO-PISCES simulations is openly accessible on the ODATIS-supported center 'Sea scientific open data publication' (https://doi.org/10.17882/72239).

Code availability

The Python module 'statsmodels' (https://www.statsmodels.org/stable/index.html) was used for linear regression and the calculation of prediction intervals. The mocsy2.0 routines were used to calculate the ocean carbonate system variables (http://ocmip5.ipsl.jussieu.fr/mocsy/). The Climate Data Operators (CDO) were used for regridding of CMIP5 model output (https://code.mpimet.mpg.de/projects/cdo/). The code for the NEMO ocean model version 3.2 is available under CeCILL license online (http://www.nemo-ocean.eu).

Extended Data: Emergent constraint on Arctic Ocean acidification in the twenty-first century

Jens Terhaar[1,2*], Lester Kwiatkowski [1,3], Laurent Bopp[1]

[1] LMD/IPSL, Ecole Normale Supérieure/PSL Université, CNRS, Ecole Polytechnique, Sorbonne Université, Paris, France

[2] Oeschger Centre for Climate Change Research and Climate and Environmental Physics, Physics Institute, University of Bern, Bern, Switzerland

[3] LOCEAN, Sorbonne Université-CNRS-IRD-MNHN, Paris, France

***Jens Terhaar**

Climate and Environmental Physics, Physics Institute

University of Bern

Sidlerstrasse 5

3012 Bern

Switzerland

jens.terhaar@climate.unibe.ch

Extended Data Table 1. The probability (%) of different year 2100 acidification extremes under RCP8.5 in the CMIP5 prior and after the application of the maximum surface density emergent constraint.

	$\Omega_{arag} < 0.75$		$\Omega_{calc} < 1.0$		pH < 7.85	
	Arctic Basin (0-bottom)	Mesopelagic (400-800m)	Arctic Basin (0-bottom)	Mesopelagic (400-800m)	Arctic Basin (0-bottom)	Mesopelagic (400-800m)
CMIP5 prior	24	51	3	23	35	83
Emergent constraint	41	88	1	37	62	100

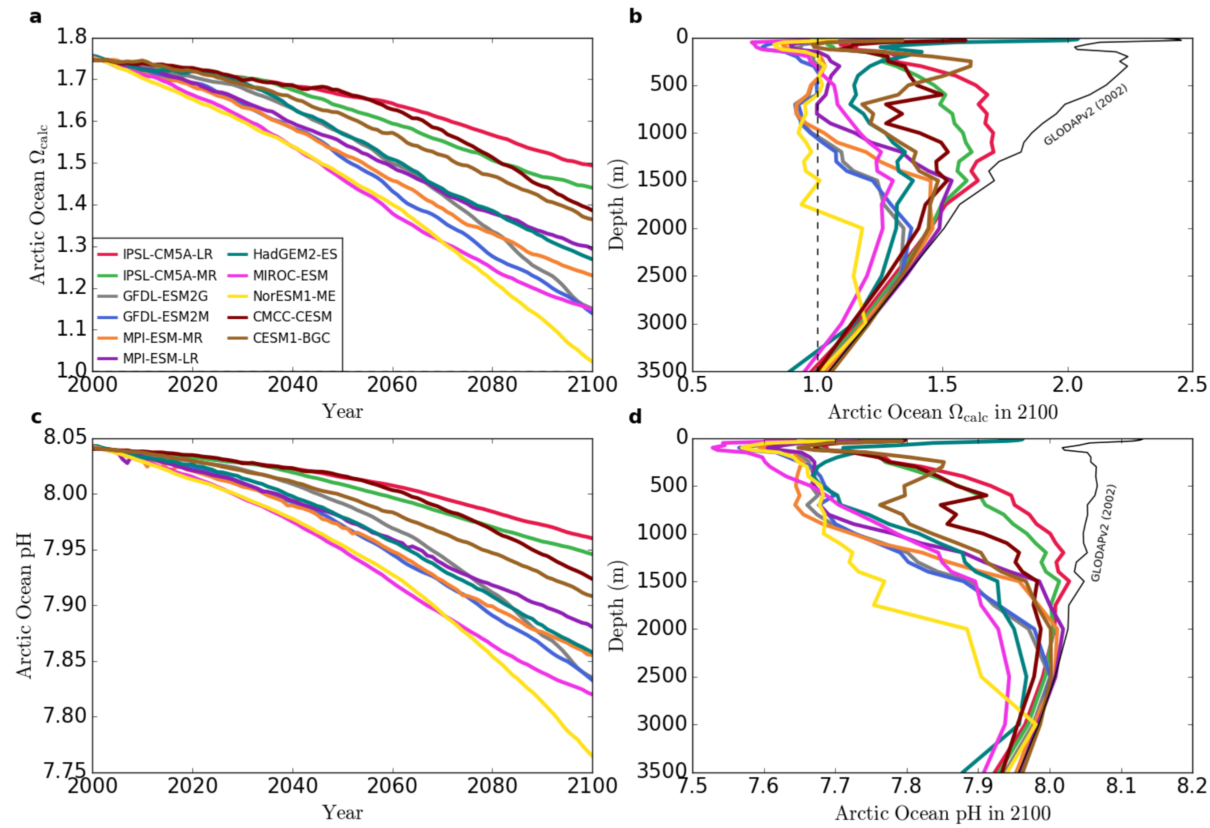

Extended Data Figure 1. Projections of Arctic Ocean calcite saturation state and pH. a, ESM projections of the twenty-first century Arctic Ocean basin-averaged Ω_{calc} and **c,** basin-averaged pH. Vertical profiles of **b,** basin-averaged Ω_{calc} and **d,** pH in 2100 for the 11 ESMs. The GLODAPv2 observational profiles of Ω_{calc} and pH for 2002 are marked as a black line in **b** and **d**.

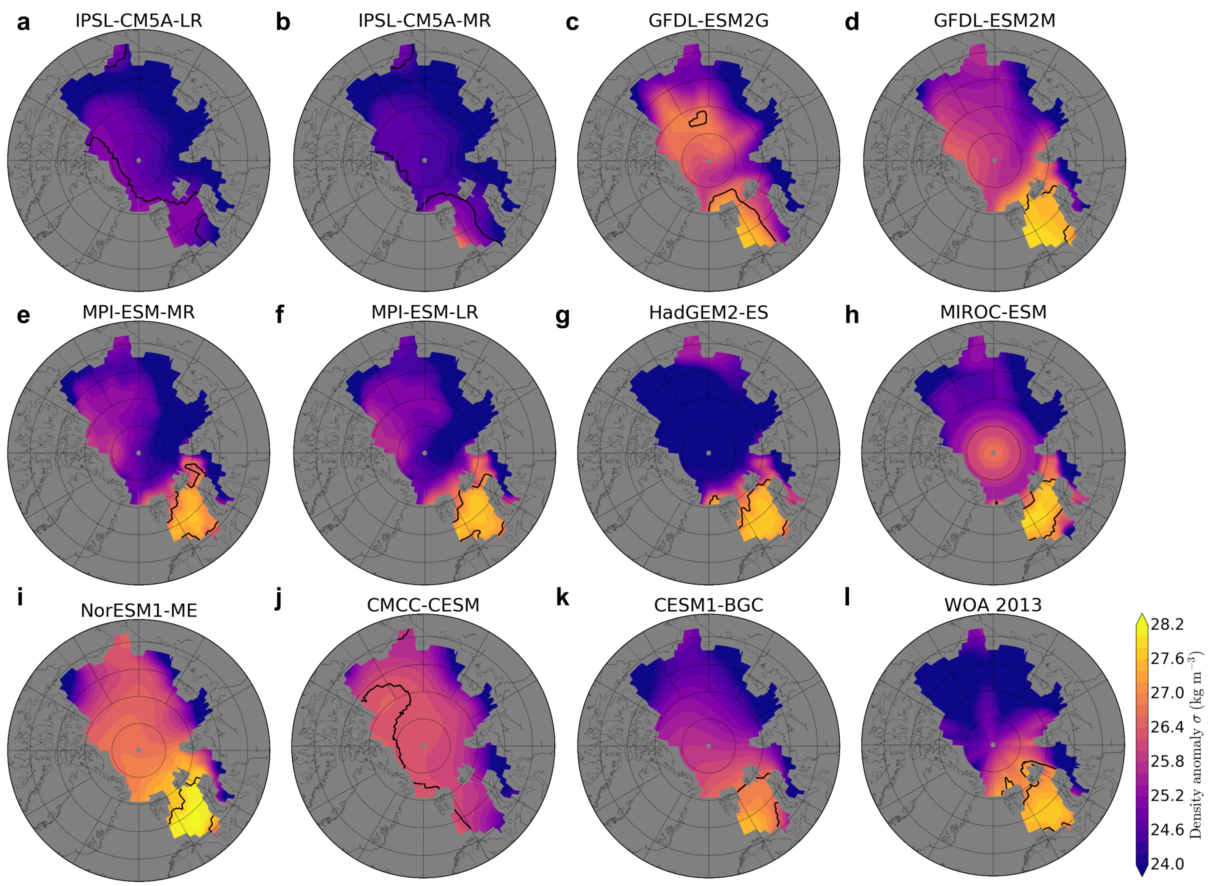

Extended Data Figure 2. Arctic Ocean surface water density. Present-day annual-mean sea surface density from **a-k,** the 11 ESMs and from **l**, World Ocean Atlas 2013 observations. Contours delineate regions that contribute to the maximum surface density as defined by the 95th percentile densities.

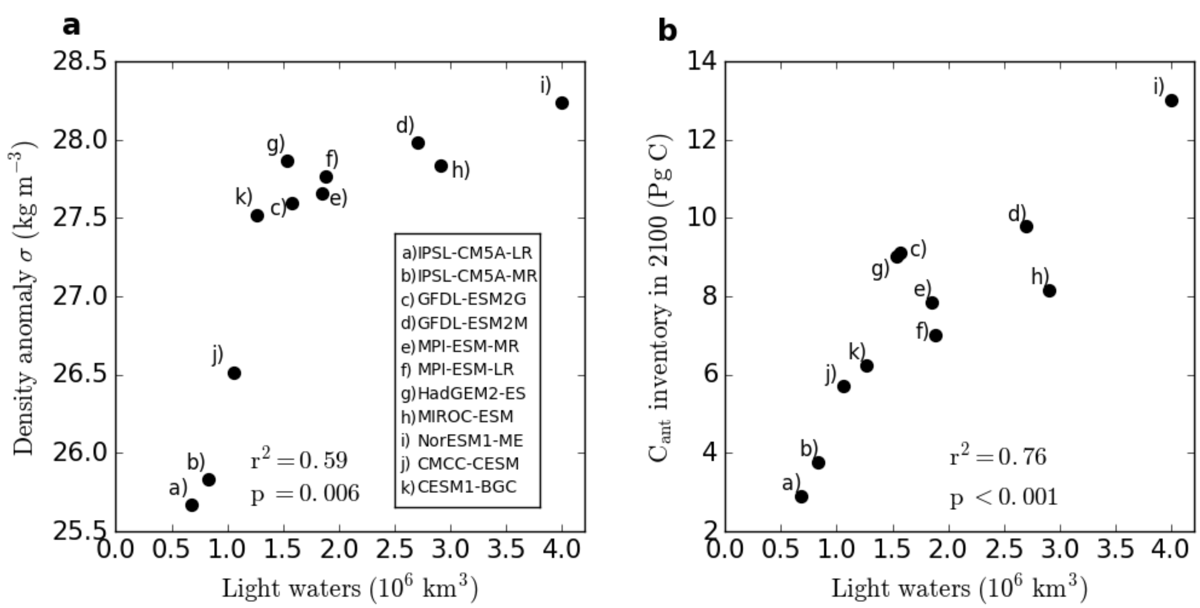

Extended Data Figure 3. Arctic Ocean present-day density anomaly and anthropogenic carbon inventory in 2100 against the volume of light waters: a, Arctic Ocean present-day maximum density anomaly and **b**, Arctic Ocean anthropogenic carbon inventory in 2100 against the volume of light waters. The volume of light waters is defined as the volume of water masses with densities below the respective maximum sea surface density (95^{th} percentile waters).

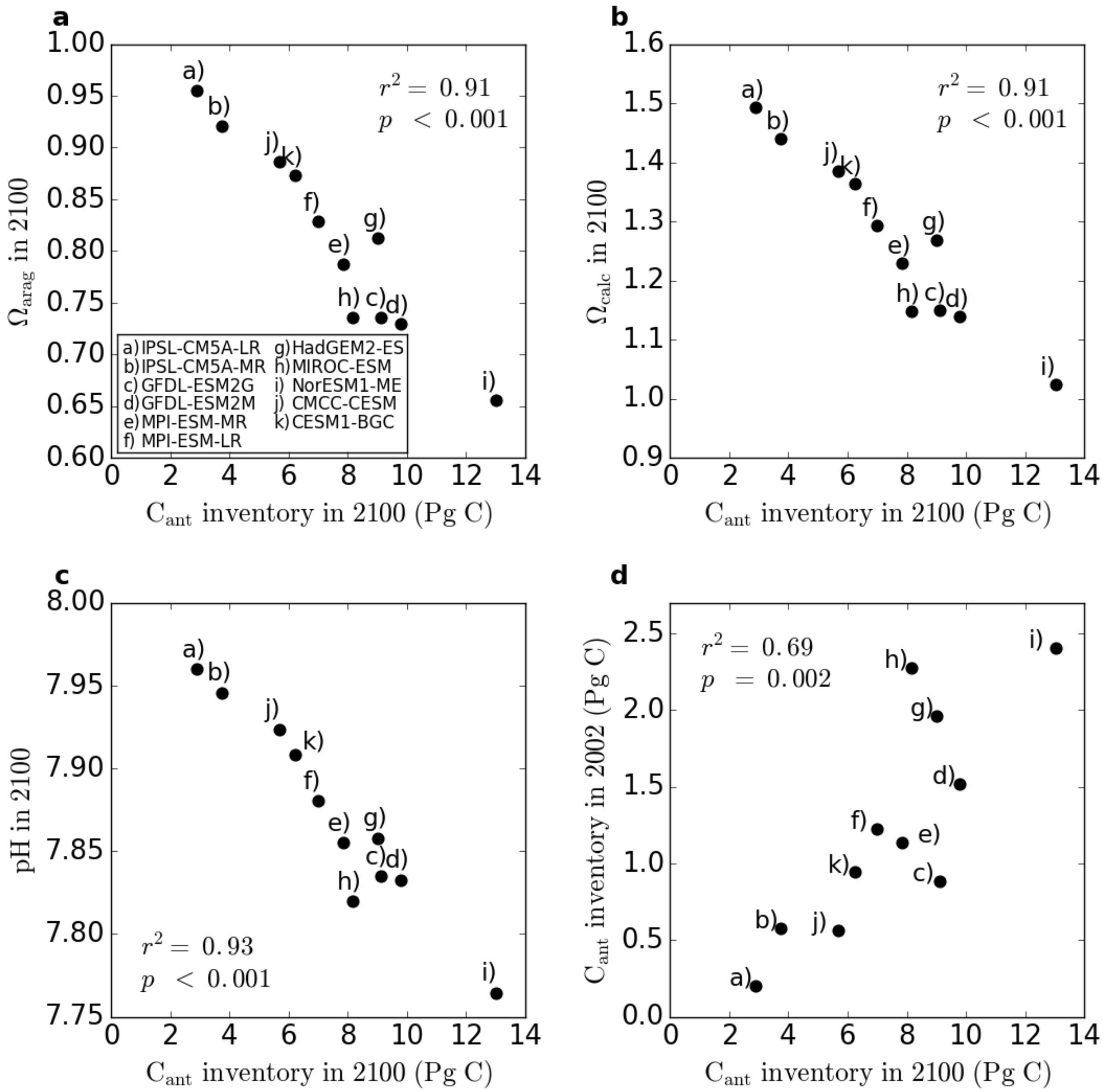

Extended Data Figure 4. Correlations between projections of the Arctic Ocean anthropogenic carbon inventory and Ω_{arag}, Ω_{calc} and pH. Arctic Ocean basin-averaged **a,** Ω_{arag} in 2100, **b,** Ω_{calc} in 2100, **c,** pH in 2100, and (d) the anthropogenic carbon inventory in 2002 against the anthropogenic carbon inventory in 2100 for the 11 ESMs.

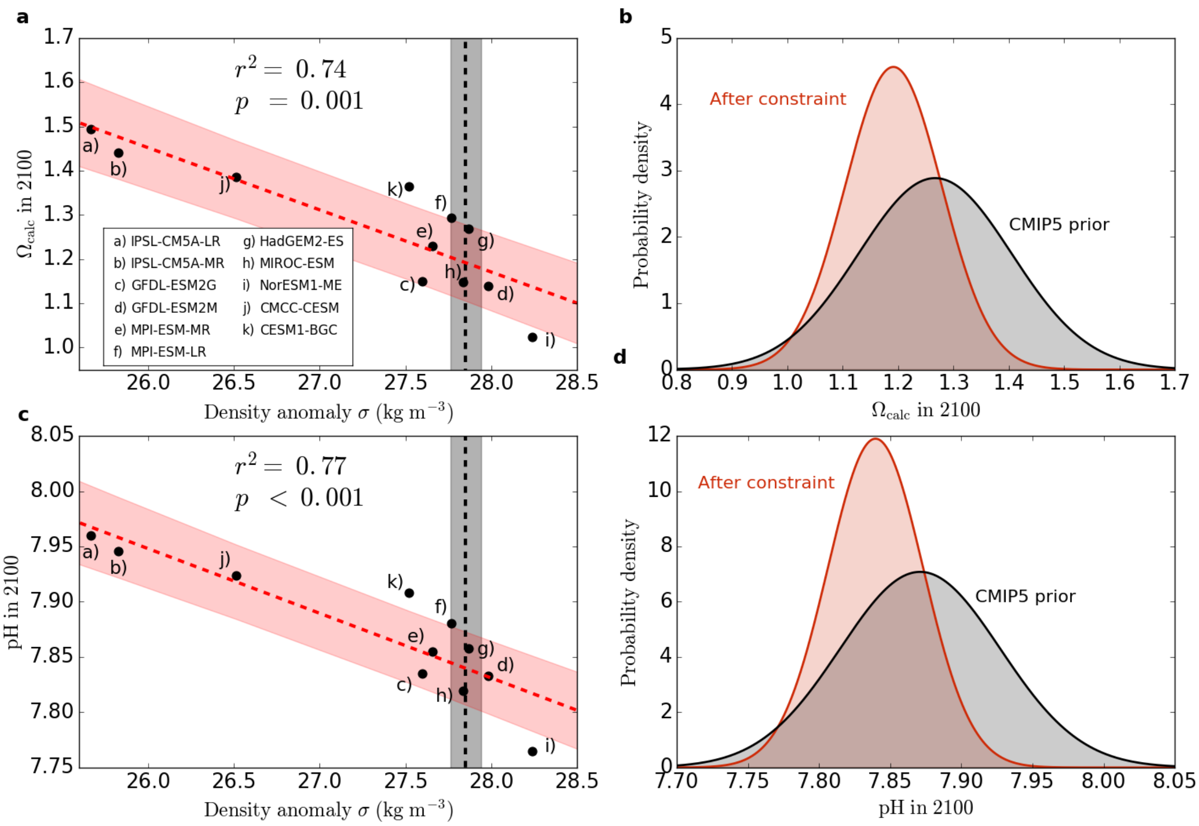

Extended Data Figure 5. Emergent constraints on projected Ω_{calc} and pH**. a,** The projected Arctic Ocean basin-averaged Ω_{calc} and **c,** basin-averaged pH in 2100 against present-day maximum sea surface density (95th percentile waters) for the ESM ensemble (black dots). Linear regression fits (red dashed lines) and the associated 68 % prediction intervals are shown, as are data-based estimates of present-day maximum sea surface density (black dashed lines) with the associated standard deviation (black shaded area). Probability density functions for the end-of-century **b,** Arctic Ocean basin-averaged Ω_{calc} and **d,** basin-averaged pH, before (black) and after (red) the emergent constraint is applied.

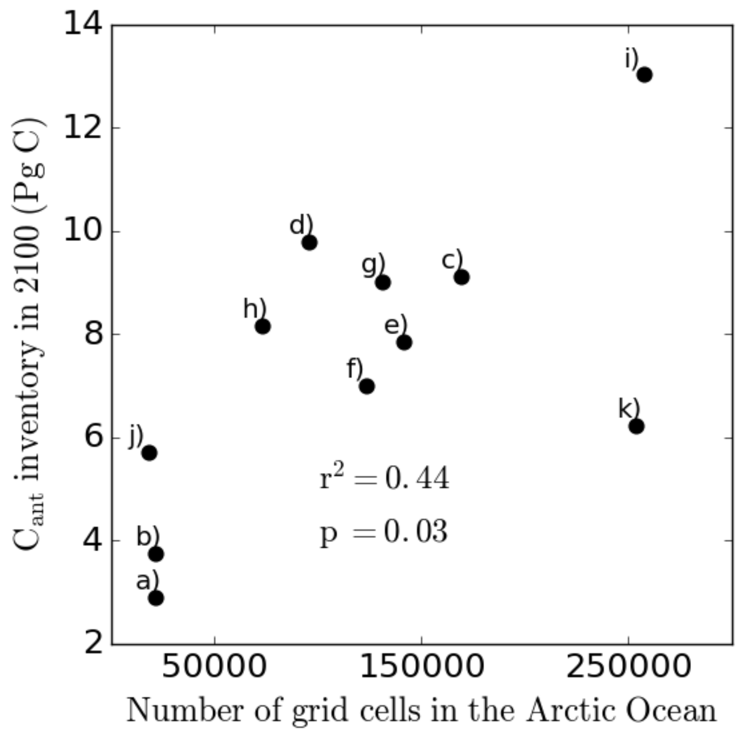

Extended Data Figure 6. Arctic Ocean anthropogenic carbon inventory in 2100 against the number of grid cells in the Arctic Ocean on the native model grid. Arctic Ocean anthropogenic carbon inventory in 2100 against number of grid cells on the native model grid in the Arctic Ocean for each of the 11 ESMs.

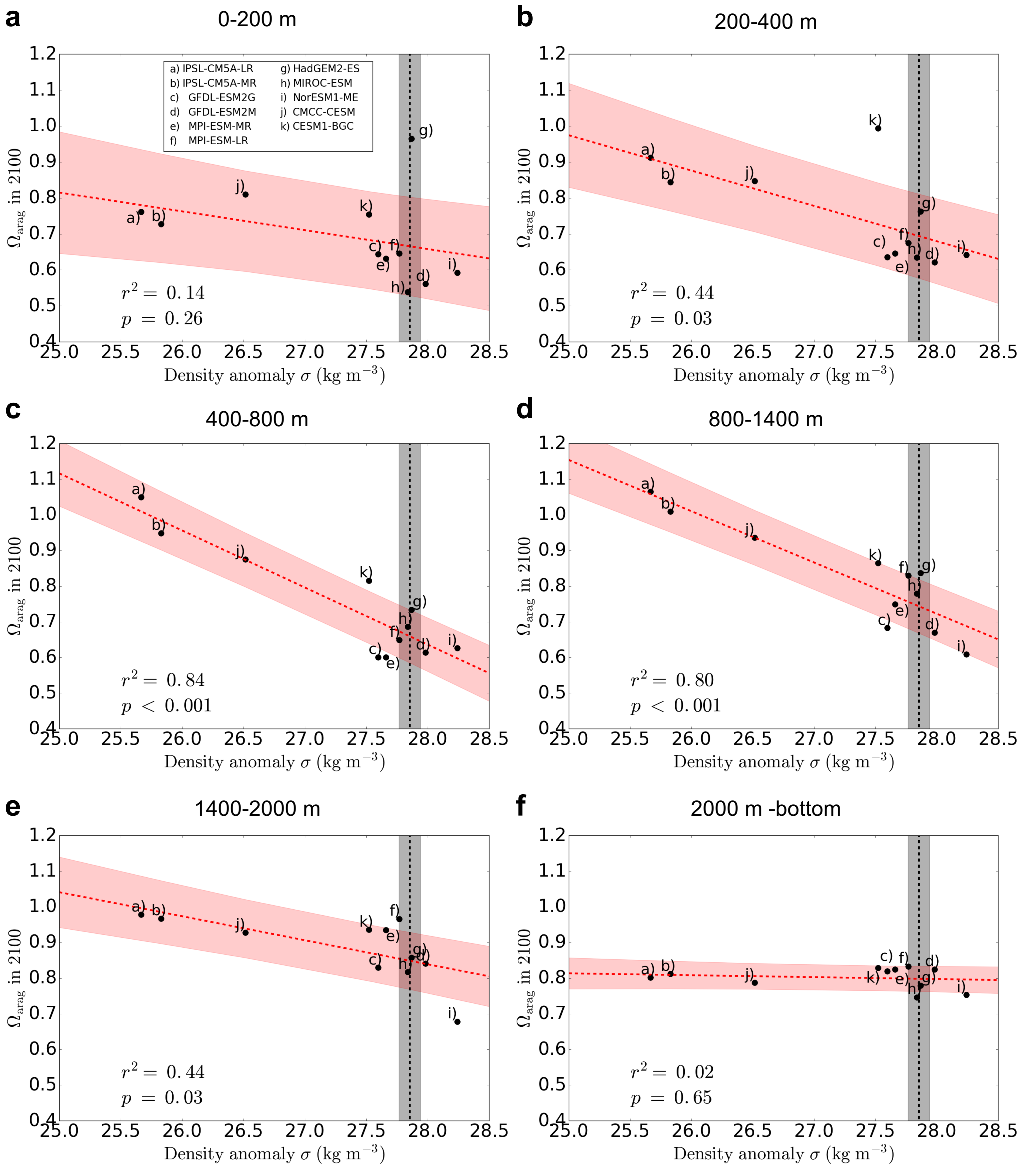

Extended Data Figure 7. Emergent constraints on future aragonite saturation state in different depth layers. The projected end-of-century Arctic Ocean Ω_{arag}, across six depth layers from **a-f**, against maximum sea surface density (95th percentile waters) for the ESM ensemble (black dots). Linear regression fits (red dashed lines) and the associated 68 % prediction intervals are shown, as are data-based estimates of present-day maximum sea surface density (black dashed lines) with the associated standard deviation (black shaded area).

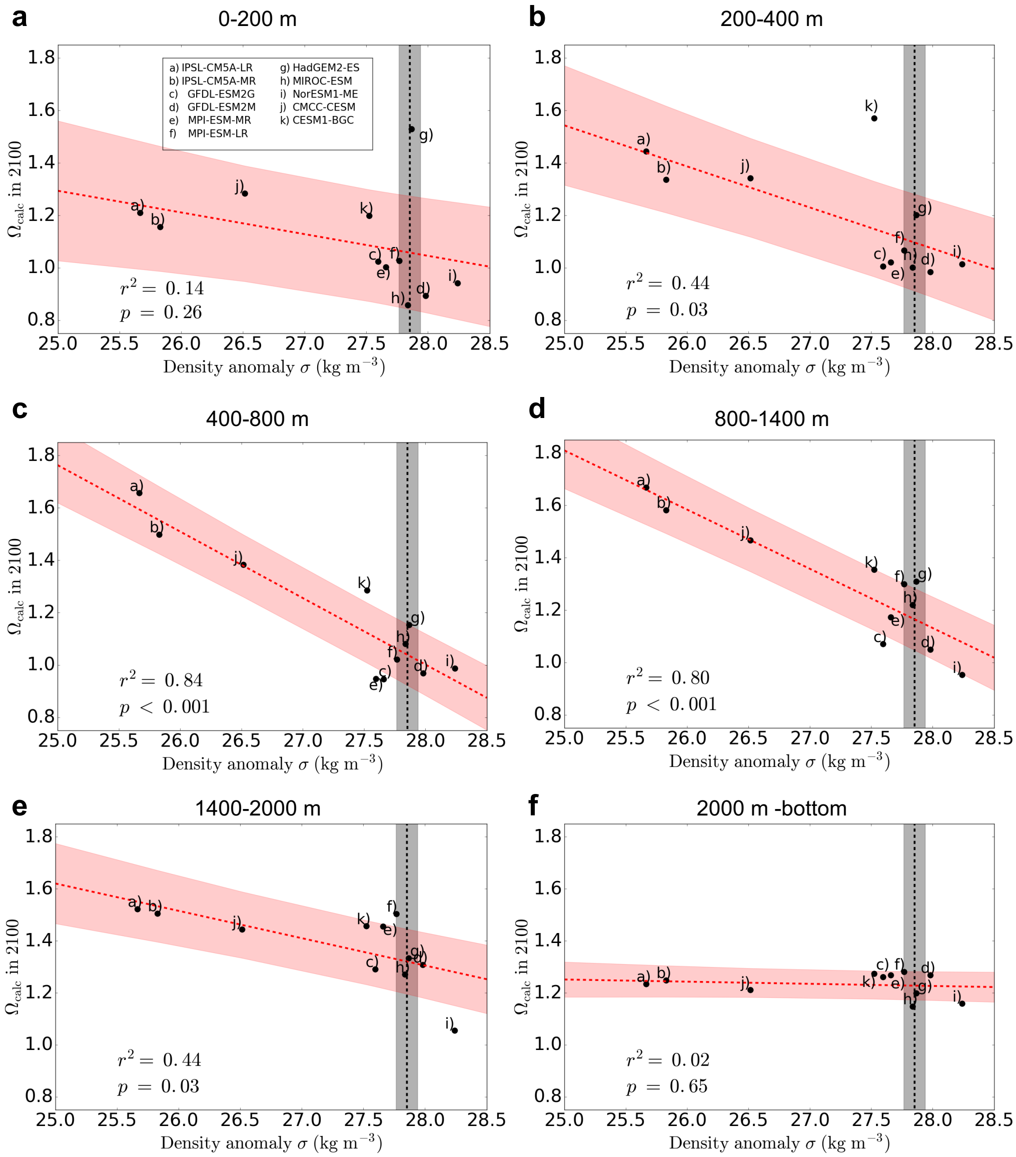

Extended Data Figure 8. Emergent constraints on future calcite saturation state in different depth layers. The projected end-of-century Arctic Ocean Ω_{calc}, across six depth layers from **a-f**, against maximum sea surface density (95th percentile waters) for the ESM ensemble (black dots). Linear regression fits (red dashed lines) and the associated 68 % prediction intervals are shown, as are data-based estimates of present-day maximum sea surface density (black dashed lines) with the associated standard deviation (black shaded area).

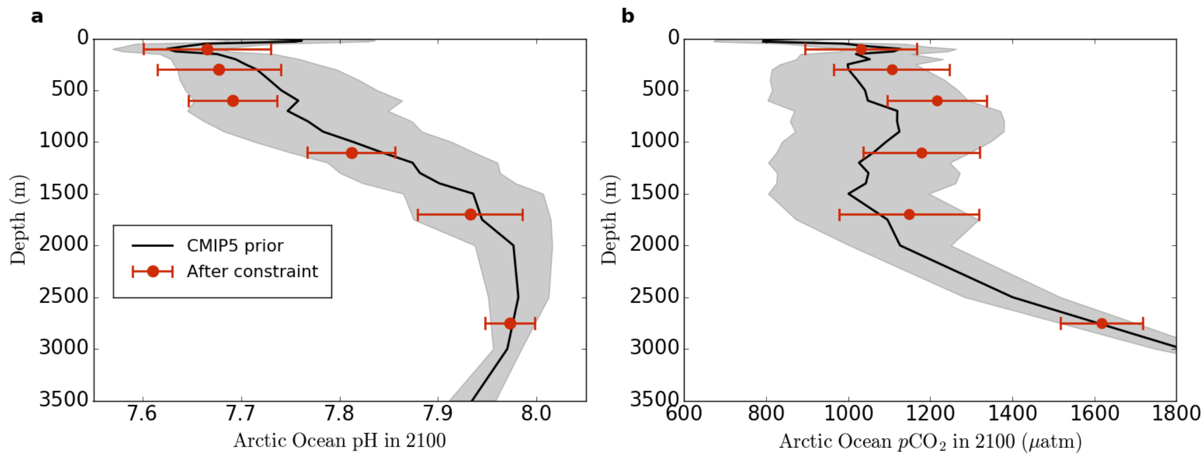

Extended Data Figure 9. Constrained end-of century Arctic Ocean vertical profiles of pH and $\boldsymbol{p}\mathbf{CO_2}$. Multi-model mean vertical profiles of basin-averaged **a,** pH and **b,** pCO_2 in 2100 (black lines) with the associated standard deviation (grey shading). Constrained estimates of pH and pCO_2 (red dots) are shown for six different depth layers (0-200 m, 200-400 m, 400-800 m, 800-1400 m, 1400-2000 m, 2000-3500 m). The constrained estimates are shown at the mid-point of each layer, with error bars representing ± one standard deviation.